



Article

# Applications of Unmanned Aerial Systems (UASs) in Oil and Gas Industry: A Proportional-Integral Based Terminal Sliding Mode Control (PI-TSMC) Approach

Amna Altaf <sup>1,†</sup>, Adeel Mehmood <sup>2,‡</sup> , Jamshed Iqbal <sup>2,3,\*</sup> , Khalid Munawar <sup>4</sup>, Ali Al-zahrani <sup>3</sup> and Anas M. Hashmi <sup>3</sup>

<sup>1</sup> Univ. Artois, UR 3926 Laboratoire de Génie Informatique et d'Automatique de l'Artois (LGI2A), F-62400, France;

<sup>2</sup> School of Computer Science, Faculty of Science and Engineering, University of Hull, HU6 7RX, United Kingdom;

<sup>3</sup> Department of Electrical and Electronic Engineering, Faculty of Engineering, University of Jeddah, Kingdom of Saudi Arabia;

<sup>4</sup> Department of Electrical and Computer Engineering, King Abdulaziz University, P.O. Box 80204, Jeddah 21589, Kingdom of Saudi Arabia.

\* Correspondence: j.iqbal@hull.ac.uk

† These authors contributed equally to this work.

Version June 8, 2023 submitted to Drones

**Abstract:** Over the last decade, Unmanned Aerial Vehicles (UAVs) have grown in popularity in various commercial and military application areas, such as photography, mining, surveillance, agriculture, medicine, and specific military uses. The usage of UAVs is increasing worldwide because they provide significant advantages in terms of reduced costs and human workload and increased efficiency and productivity in almost every field of life. The oil and gas industry, being one of the world's largest industries, is keen to adopt this technology in order to revolutionize its operations. This ambition can only be achieved by benefiting from cutting-edge technological advancements. The oil and gas industry owns expensive and widely spread assets; any faults in this complex infrastructure network may result in accidents and/or huge losses. Real-time monitoring and primitive measures based on fault propagation analysis will limit some of the losses. Intelligent Unmanned Aerial Systems (UAS) have the potential to offer risk-free, time-optimal, and cost-effective real-time monitoring solutions with minimal human intervention. The current research discusses various trends in the applications of UAVs in the oil and gas industry, such as operational support, environmental safety, security features, and corporate and social responsibility. Moreover, the Proportional-Integral based Terminal Sliding Mode Control (PI-TSMC) design of an underactuated quadcopter system is proposed to evaluate its tracking performance. UAVs integrated with cutting-edge technologies, such as IoT sensors, machine learning and artificial intelligence techniques for rapid improvement in the transformation of the oil and gas industry are also discussed in this paper. With a low-cost, efficient, and safe line of action, UAVs produce cost-effective and accurate results in routine maintenance, operational tasks, and response to emergency-based scenarios. It is expected that the wider dissemination of the instrumental role of UAVs in the oil and gas sector will contribute to further developments and stimulate more collaborations among professionals.

**Keywords:** Unmanned Aerial Systems (UAS); Nonlinear Control Design; Drones; Surveillance

## 1. Introduction

The oil and gas industry is continuously seeking ways to leverage cutting-edge technological advancements to gain a competitive edge and address emerging challenges [1–4]. Technology is a multiplier and the augmented impact of the leading technological trends, including, but not limited to, AI (Artificial Intelligence), cloud models, sensors, and data analytics are the key factors for exponential growth in the industry [5–8]. Among the remarkable products of the Industry 4.0 Revolution, unmanned aerial systems (UASs) and unmanned aerial vehicles (UAVs) have emerged as a crucial innovation with significant potential [9–12].

UAVs, commonly referred to as drones, are remotely operated aircraft that operate autonomously or under partial human control from a ground station. In recent years, UAVs have gained popularity in both industry and research platforms, due to their far-reaching potentials in challenging tasks [13]. They offer numerous competitive advantages over traditional manned aerial vehicles, including their compact size, versatile structure, cost-effectiveness, and operational features such as vertical takeoff and landing and hovering capabilities. These characteristics make UAVs an attractive solution for a wide range of applications across various industries, including academia, reporting and journalism, traffic control, emergency response, environmental monitoring, healthcare, security, military operations, and surveillance [14–24].

This paper focuses on the application of UAVs in the oil and gas industry, which faces numerous challenges in maintaining high production levels, ensuring safety, and minimizing environmental risks [25]. With the global oil industry comprising extensive transmission pipelines covering approximately 3 million kilometers and generating billions of dollars in revenue, the need for effective solutions to detect and prevent equipment failures, leaks, and potential accidents has become paramount [26]. The failure of equipment (breakage or leaks) can result in tragic incidences like Exxon Valdez and Deepwater Horizon oil spills etc. [27]. The volume of these transmissions is increasing continuously; therefore, the need for security for this infrastructure needs a cutting-edge solution. Early detection of damages or anomalies in pipeline infrastructure is crucial for minimizing hydrocarbon loss and mitigating the environmental impact [28,29]. Traditional inspection methods often involve shutdowns or visual inspections by helicopters, which are costly, time-consuming, and limited in their perspectives. The advent of UAVs has revolutionized pipeline inspection by offering a cost-effective, efficient, and safe alternative [30]. The UAS using UAVs is a highly cost-effective, efficient, and safe solution for fault detection since there is no disruption in normal operation and there is no special need to shut down the facility for inspection. This is particularly beneficial for online flares where traditional inspection is done by shutting down the facility for visual inspection. Before the advent of UAVs, construction contractors used to hire helicopters to visually inspect major sites like Cushing, Oklahoma—the Pipeline Crossroads of the World [31]. This method had two major drawbacks: first, it was notoriously expensive; secondly, the visual data comprised very limited images from specific perspectives [32]. However, with the use of UAVs, the required images are captured and processed very effectively: an entire installation expanded at an area of 18 acres can be covered in only 15 minutes [33].

By employing UAVs, the oil and gas industry can achieve real-time, aerial data capture, enabling the early detection of damages or leaks without disrupting normal operations [30]. UAVs equipped with high-resolution cameras and advanced image processing algorithms can capture comprehensive aerial imagery of large-scale infrastructure, which can be converted into meaningful data for predictive analysis and on-the-spot decision-making [27,34]. The unique maneuvering capabilities of UAVs, facilitated by robust nonlinear controllers, allow them to hover, maneuver at high degrees, carry different payloads, and swiftly navigate challenging weather conditions [35–37]. The aforementioned characteristics can be achieved by designing robust nonlinear controllers for the UAV [38–42]. In this paper, we propose the use of a Proportional-Integral based Terminal Sliding Mode Control (PI-TSMC) approach to enhance the maneuvering capabilities of a quadcopter UAV.

The UAVs can be customized and designed as per the requirement, and they can possess the unique ability to operate in challenging weather conditions without getting affected [43,44]. They

have strong attenuation characteristics against the adverse undesired torques generated due to the reverse spinning or rotation of the aircraft propellers. Besides this, many researchers have also proposed various control design techniques, such as terminal sliding mode control [45], deep and reinforcement learning-based control [46], and fuzzy control [47]. Due to the sophisticated control design, the UAVs can hover with the distinctive capability of maneuvering at high degrees, carry distinct weights as payloads, and have much more flexible and faster movement than traditional aircraft. To further enhance the maneuvering capabilities of drones, a robust Proportional-Integral based Terminal Sliding Mode Control (PI-TSMC) technique has been presented for a quadcopter UAV in this work, which has both the additive advantages of PI control and TSMC control.

Two types of UAV platforms are used for the inspection: fixed-wing and rotary-wing aircraft. Both have their own merits and demerits. The fixed-wing UAVs are suitable for long endurance tasks and are very stable in extreme weather conditions due to being energy-efficient [48–50]. On the contrary, rotary-wing aircraft are not very energy-efficient and are less suitable for long surveillance projects, and typically their flight time is limited from 20 to 60 minutes. However, such aircraft has outstanding maneuverability and landing and takeoff convenience without needing large open spaces since it can hover, take off, and land vertically [51]. The phenomenon is known as vertical take-off and landing (VTOL), and this type of UAS gets the apparent advantage of deploying the sensor closest to the source; hence, it is preferred for field operations with runway limitations. Henceforth, a rotary-wing quadcopter drone has been considered for control design and data acquisition in current research. Nevertheless, in both cases, the selected models' frame may require modification to carry the trace gas detection system to be deployed [52].

The type of data and information obtained from the mission depends upon the type of sensors carried by the UAV Platform. The sensors have two main types: active and passive, depending upon the energy eliminated from the source object [53]. Active sensors emit their energy themselves in the form of radiation, whereas passive sensors rely on solar energy for illumination. The selection of sensors among active sensors (visible, multispectral, SWIR, thermal IR, video, stereo cameras, and gas IR camera) and passive sensors (lidar, radar, laser gas detector, and laser fluorosensor) also defines the lifting and carrying characteristics needed by the UAV Platform [54,55]. In addition to the use of aircraft and sensors, a series of auxiliary equipment has also been employed in order to make the mission successful [56]. The most commonly used systems and elements in this domain include position and navigation system, a communication medium, and autonomous flight-supporting software [29,57]. A comparison of different off-the-shelf vertical take-off and landing (VTOL) quadcopter UAVs is presented in Table 1. The prices quoted in the table were acquired at the time of writing this paper.

Additionally, the selection of sensors plays a crucial role in capturing relevant data during UAV missions. Active and passive sensors, depending on their energy emission source, offer different capabilities for data collection. Active sensors emit their energy, while passive sensors rely on solar energy for illumination. The selection of sensors, such as visible, multispectral, thermal, or gas detectors, determines the payload and lifting characteristics required by the UAV platform. Moreover, auxiliary equipment, including position and navigation systems, communication mediums, and autonomous flight-supporting software, contribute to the success of UAV.

Section 2 presents the infrastructure of the UAV system and proposed methodology for the research work. Various case studies of the implementation of UAVs based projects in industry are discussed in Section 3. Section 4 presents the nonlinear control design of quadcopter and the performance analysis of various simulations carried out in this project. Finally, discussions, challenges and conclusions are presented in sections 5 and 6.

## 2. UAS Architecture & Proposed Infrastructure

The UAV technology is based on the concept of flying an aircraft without a human pilot, i.e., an architecture based on airframe and ground control station computer systems connected through a wireless communication network combining GPS, sensors, and computer-based servers to eliminate

**Table 1.** Comparison of different off-the-shelf vertical take-off and landing (VTOL) quadcopter UAVs.

S. No.	Model	Weight (g)	Properties	Pay load capacity (g)	Flight time (min)	Max speed (km/h)	Price (\$)
1	Phantom 3 Advanced	1280	- 4K video, 12 megapixel photo camera - Integrated 3-axis stabilization gimbal	1200	23	57.6	1461
2	Mavic 2 Pro	907	- Hasselblad L1D-20c 20 megapixel photo camera - Sensors for vision(5), GPS and GLONASS, one ultrasonic range finders pair	1137	31	65	1599
3	Autel Robotics - EVO II Pro Professional Drone	863	- CMOS 16 megapixel photo camera - 12 sensor omnidirectional obstacle avoidance coupled with a dual-core processor	1000	40	72	1799
4	Phantom 4 professional	1388	- 1 inch, 20 megapixel CMOS camera - Extended maximum transmission range of 7km - Dual rear vision sensors and two range imaging cameras for obstacle sensing	907	30	72	1499
5	Parrot - ANAFI Extended Drone	322	- CMOS 21 megapixel camera with 24fps video - 180° tilt gimbal, capturing and 3-axis image stabilization	-	32	50	899
6	Yuneec - Mantis G	505	- Improve maneuvering, and the voice control and facial detection features - CMOS 13 megapixel camera with 30fps video	-	33	25	699
7	Ryze Tech - Tello Boost Combo	82	- CMOS 5 megapixel camera with shoots 720HD video at 30 fps - Ensures safe landing even if the connection is lost	-	13	29	149
8	Hubsan Zino Pro	700	- 4K ultra high definition 8-megapixel camera with 30fps video - 3-axis gimbal camera stabilizer for stabilizing the camera during high-speed/ GPS /follow me/headless mode /auto return to home	-	23	60	379
9	Sky Rider - Foldable Quadcopter	80	- Foldable Quadcopter with Remote Controller (Android and iOS-compatible)		6-8		69
10	Protocol Drone Model:6182-3MXB	750	- 0.4-megapixel camera with shoots 480p video - Smartphone mount, USB cable charger	-	5	-	79

the need for human intervention as an aviator in the flight [58]. The component in a UAS enables autonomous operations controlled from a ground station, and the parameters like size, type of sensors, and configuration of entities vary from application to application. However, the system highly relies on the enabling technological entities [59,60].

- **Entities:** UAV is an autonomous flying body, automatically piloted using a flight control computer embedded in the device. A typical UAV platform includes digital cameras interfaces against a geospatial processor [59,61]. The georeferenced data, typically in the form of images, are transmitted through a flexible data networking switch fabric, making the system configuration simple and extensible. The mission of a UAV is executed over a predetermined flight plan and captures data using multiple types of sensors, such as GPS, accelerometers, gyros, and pressure sensors [58]. UAS is a complex UAV-based system with the following main entities that work in a coordinated framework for generating valuable information related to the target. Fig. 1 presents a graphic representation of the system [62].
- **UAV Airframe:** The UAV is a lightweight aircraft that is aerodynamically efficient and comprises a stable platform. Since the UAV is autonomous, it has limited space for avionics support and no space for a human operator inside the aircraft [63,64].
- **Flight Computer:** It is the main component of a UAV, and as the name suggests, it controls the flight of a UAV. It uses various sensors to collect the aerodynamics data for directing the flight of the aircraft automatically along the predetermined flight plan through the control surfaces in the UAV airframe [60].
- **Payload and Payload Controller:** The payload comprises a set of sensors (including but not limited to TV cameras and thermal and infrared sensors). The payload is deployed to capture data to be transmitted to the ground station in raw or partially or fully processed form [65]. The payload controller is another computer system used to control the payload's operations and the sensors included in it. The operation of the payload controller is aligned with the flight plan of the UAV and the mission of the UAS [61,66].
- **Ground Station:** This is also known as the base station. It comprises an on-ground computer-based system aimed at monitoring the overall mission and ultimately controls the operation of both UAV and its payload [62,66].
- **Communication Network:** The communication infrastructure of a UAS is a mix of multiple communication techniques and mechanisms, such as modems, satellite communication, and microwave link. The objective is to provide an uninterrupted, high-availability communication link between the UAV airframe and the ground station [58,67]. Modern UAS technologies offer a wide range of solutions for each component in the UAS, providing highly flexible and cost-efficient, mission-specific infrastructure for various applications [67,68].

### 2.1. Platform Setup

A ground-based control computer is employed for the triggering of camera operation. As the image is captured, stored, and prepared for transmission, the metadata is attached to the image, including the information on camera setting parameters and geospatial settings like position and altitude [66]. This real-time data is transmitted to the ground station through a wireless network connection. Due to technological advancements, UAVs can capture and transmit large-megapixel data, images, and metadata through streaming. In most setups, the ground station has two separate computer systems, one handling the flight and the other handling the image-related operations. However, despite the decoupling, the two computers exchange real-time information [68]. The requirements of the operation and the flight path details are pre-programmed in software, commonly known as mission planning software, by the human operator at the ground station [44,69]. The autopilot is fed with the necessary information to direct and control the aircraft's flight during the mission/operation.



**Figure 1.** UAV platform based on remote sensing techniques.

The sensing capabilities of a UAS can be amplified by combining multiple cameras into a unique assembly. Various remote sensing techniques are particularly applied in this domain by using multispectral imaging devices, infrared and thermal cameras, and spectroscopy [64,70,71]. For instance, a modular mounting scheme can be implied on a single camera frame, allowing multiple camera modules to be configured on a single frame to best suit the requirements of a mission. The shutter of these cameras must be synchronized, and the optical axis of all the cameras should be parallel to each other to operate simultaneously [72]. Using this type of assembly, various images, such as a mix of color, monochrome, and false color images, of the same target can be acquired; afterward, a single high-quality, detailed image of the target can be generated by employing digital image processing techniques [60,73]. UAVs are usually operated in semi-autonomous mode, which involves manual control. A robust control law is more desirable to make the UAV fully autonomous because it can incorporate uncertainties [42]. In the next section, different applications and case studies of UAVs in the oil and gas sector are discussed.

### 3. Application in Oil and Gas Sector

The petroleum industry holds a distinctive significance in modern world operations and has become a major energy source all across the globe ever since the modern discovery of petroleum in the last quarter of the 19th century [74]. The function of petroleum has been evolving over time, and with the advent of the oil and gas sector, the industrial advancement in the world has also staggered, and over the years, this industry has attained a far-reaching influence over the activities of individuals as well as strong impact on the economy of the oil exporting countries and oil-importing countries and the business and economy of the world at large [75,76].

The oil and gas infrastructure, including the exploration, production, refinement, storage, and transportation facilities, are subject to multiple operational challenges [77,78]. The nature of these



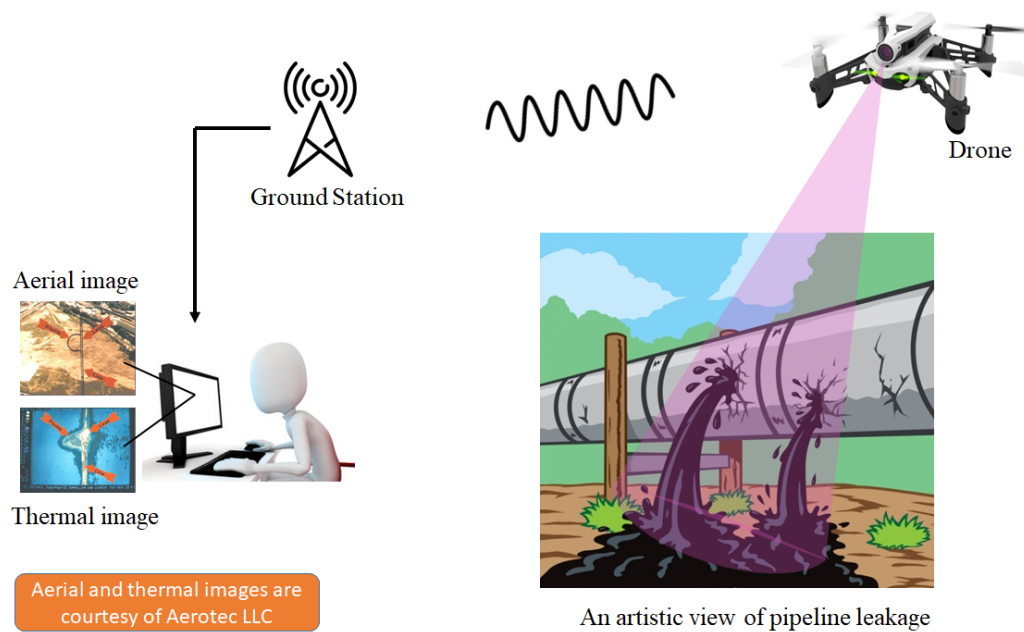


**Figure 2.** Simplified conceptual diagram presenting a novel infrastructure monitoring and fault detection/analysis system.

challenges varies from operational nature of the function a company performs; from upstream to midstream and downstream companies. With the advancement of technology supplemented by the rapid improvement in IoT (Internet of Things), AI, and big data technologies, the transformations in the oil and gas operations have also evolved over the years [79]. This particularly includes the advancement in techniques used for the inspection and monitoring of the physical machinery, which is usually spread over huge landscapes [80]. Therefore, various large oil and gas operating organizations worldwide imply UAVs for surveillance and monitoring of the enormous infrastructure [27]. UAVs are particularly preferred due to their distinctive advantages over the traditional approaches that help organizations comply with their regulatory requirements safely and comfortably. The aerial monitoring offered by these remotely operated rugged birds is effort-free, and they can maneuver easily around the enormous infrastructure comprising newly constructed sites, rigs, plants, underdecks, and a widely spread network of pipelines. Fig. 2 illustrates the conceptual view of oil spill detection with the help of UAVs. This, in turn, helps the management to put their time, effort, and cost into taking proactive approaches for detecting fault or leakage instead of relying on reactive maintenance measures and compliance. These UAVs are cutting-edge devices that are becoming indispensable for oil and gas companies contributing to transforming current industry practices. Various UAV manufacturing companies are also collaborating with the oil and gas sector to explore applications that can use the realistic insights gathered by these devices. Furthermore, the elaborated advantages of UAVs are presented in the next section.

### 3.1. Case Studies

Drones use has been started in the oil and gas sector as a cost-effective and flexible way to manage inspections. UAVs use in oil and gas companies improve the quality of investigations, provide increased safety for workers, and reduce the expensive cost linked with manual inspection [25]. British Petroleum (BP), one of the first adopters of drones, conducted their pilot studies at its oil fields in 2006, in Alaska. Their studies examined effectiveness of monitoring gravel road conditions via drones. Using drones helped safeguard efficient and safe movement of trucks during oilfield equipment supply at the production site [25,81]. The oil and gas drone service market is fragmented, and it is dominated by companies such as Terra Drone, Viper Drones, Precision Hawk, and Cyberhawk Innovations Limited,

**Table 2.** Different business cases of UAVs in oil and gas.

S.No	Company Name	Services	Software	Application Domain	Business Cases
1	Precision Hawk	Monitors the pipeline right-of-ways, inspects well sites, manages oil and gas assets	Precision Analytics Energy	Upstream, Mid Stream, Downstream	skylogic research
2	Airobotics Ltd	Provides an end-to-end, fully automatic solution for collecting aerial data and gaining invaluable insights.	Drone developer software	Upstream, Mid Stream, Downstream	NA
3	Cyberhawk Innovations Limited	provides aerial inspection and surveying by using Remotely Operated Aerial Vehicles (ROAV).	iHAWK	Upstream, Downstream	Kinsale Energy, Ireland
4	Sky-Futures Limited	Experience in drone-based inspections of oil and gas assets, provides an image analysis and mission planning platform together, inspection of wind assets, service providers of civil infrastructure such as bridges, ports, and transportation infrastructure	Inspection	Upstream, Downstream	NA
5	Sharper Shape Inc.	Provides a transformative T&D inspection solution, that adapts to each utility's specific needs, digitization efforts and existing processes	Sharper CORE	Upstream , Midstream	NA
6	Phoenix LiDAR Systems	Phoenix LiDAR Systems builds custom, survey-grade laser mapping systems, and automation software for flight planning, acquisition, and post-processing	PLS spatial explorer, PLS spatial lighthouse	Upstream, Midstream	NA
7	Viper Drones	Specialized drones with sophisticated thermal and optical imaging sensors for oil and gas industry, manufacturing, building, utility, and industrial inspections, spraying, surveillance, and surveys.	professional thermal reporting	Upstream and iidstream systems, Downstream	NA
8	SkyX Systems Corporation	Oil and gas pipeline inspection, long-range UAV missions, VTOL transitions to forward flight, precision takeoffs and landings, interchangeable sensors, and long-range flight with remote charging stations	Theskyx professional	Upstream, Mid Stream, Downstream	SAIGONTEL, Vietnam
9	Terra Drone Corporation	Drone, software, survey, inspection, UTM, UAV, and mapping	UAV software, customized software, lot software	Upstream, downstream	Chevron , Pacific Indonesia

among others. Some leading oil and gas companies using drone technology as stated by GlobalData are mentioned in Table 2. In the next section, the control design of a quadcopter UAV is presented in detail.

#### 4. Nonlinear Control Design of Quadcopter

The mathematical model of a quadcopter system can be obtained using Euler–Lagrange and/or Euler–Newton equations of motion. The model used in this research has 12 states and four control inputs. The outputs of the system are its position and orientation in 3D space [38]. Since the quadcopter is an underactuated coupled system, it is first transformed into the regular form [46]. The overall state-space model of a quadcopter after transformation can be expressed as follows:

$$\left. \begin{aligned} \dot{z}_1 &= z_2 \\ \dot{z}_2 &= -g + (\cos \vartheta_1 \cos \varphi_1) b_0 U_1 + \Delta_z \end{aligned} \right\} \quad (1)$$

$$\left. \begin{aligned} \dot{\psi}_1 &= \psi_2 \\ \dot{\psi}_2 &= a_5 \vartheta_2 \varphi_2 + b_3 U_4 + \Delta_\psi \end{aligned} \right\} \quad (2)$$

$$\left. \begin{aligned} \dot{\rho}_1 &= \rho_2, \\ \dot{\rho}_2 &= g B_\rho \\ \dot{\varphi}_1 &= \varphi_2 \\ \dot{\varphi}_2 &= a_1 \psi_2 \vartheta_2 + a_2 \bar{\omega} \vartheta_2 + b_1 U_2 + \Delta_\phi \end{aligned} \right\} \quad (3)$$



$$\left. \begin{aligned} \dot{h}_1 &= \dot{h}_2, \\ \dot{h}_2 &= gB_h \\ \dot{\vartheta}_1 &= \vartheta_2 \\ \dot{\vartheta}_2 &= a_3\psi_2\varphi_2 + a_4\bar{\omega} \varphi_2 + b_2U_3 + \Delta_\theta \end{aligned} \right\} \quad (4)$$

where  $b_0 = b/m$ ,  $b_1 = bl/I_x$ ,  $b_2 = bl/I_y$ ,  $b_3 = 1/I_z$ ,  $a_1 = (I_y - I_z)/I_x$ ,  $a_2 = I_R/I_x$ ,  $a_3 = (I_z - I_x)/I_y$ ,  $a_4 = -I_R/I_y$ ,  $a_5 = (I_x - I_y)/I_z$ ,  $B_h = (\sin \psi \sin \varphi + \cos \psi \sin \vartheta \cos \varphi) / (\cos \vartheta \cos \varphi)$  and  $B_\rho = (\sin \psi \sin \vartheta \cos \varphi - \cos \psi \sin \varphi) / (\cos \vartheta \cos \varphi)$ .

Here, the system (1-4) is demonstrated in the form of a decoupled system.

#### 4.1. Fast PI-TSMC Design

In this section, a PI-TSMC design technique has been presented for both the fully actuated and underactuated subsystems of the quadcopter. The objective is to design a robust controller that aims to achieve the complete flight trajectory of the quadcopter in finite time considering the uncertainties in the system.

##### 4.1.1. Control Design of the Underactuated Subsystem

To design the control law of the underactuated subsystem presented in (3) and (4), it is important to mention that these equations have similar dynamic structures. The objective is to steer the states and the sliding mode to their respective equilibria; therefore, the PI-TSMC surface is defined as follows:

$$s_\rho = \dot{e}_\rho + \alpha_\rho e_\rho + \beta_\rho \int_0^t |e_\rho|^{\chi_\rho} \text{sign}(e_\rho) d\tau, \quad (5)$$

where  $e_\rho = \rho_1(t) - \rho_{ref}(t)$  is the tracking error, the constants  $\alpha_\rho > \beta_\rho > 0$  are the positive design parameters, and  $\chi_\rho = q_\rho / p_\rho$  such that  $q_\rho$  and  $p_\rho$  are the positive odd integers [82]. The first derivative of (5) w.r.t. time can be written as

$$\dot{s}_\rho = \ddot{e}_\rho + \alpha_\rho \dot{e}_\rho + \beta_\rho |e_\rho|^{\chi_\rho} \text{sign}(e_\rho) \quad (6)$$

and the second derivatives of (5) can be written as

$$\ddot{s}_\rho = \ddot{e}_\rho + \alpha_\rho \ddot{e}_\rho + \chi_\rho \beta_\rho |e_\rho|^{\chi_\rho-1} \dot{e}_\rho, \quad (7)$$

where  $\dot{e}_\rho = \dot{\rho} - \dot{\rho}_{ref}$  and  $\ddot{e}_\rho = \ddot{\rho} - \ddot{\rho}_{ref}$ .

In the internal dynamics block of (3),  $g$  and  $B_\rho$  are the positive constant and the state function, respectively.  $B_\rho$  is treated as a virtual control input here. The main objective here is to maintain the following structure:

$$\begin{aligned} \dot{e}_{1\rho} &= e_{2\rho} \\ \dot{e}_{2\rho} &= -\dot{e}_{1\rho} - \alpha_\rho e_{1\rho} - \beta_\rho \int_0^t |e_{1\rho}|^{\chi_\rho} \text{sign}(e_{1\rho}) d\tau. \end{aligned} \quad (8)$$

This can be achieved by choosing

$$gB_\rho - \ddot{\rho}_{ref} = -s_\rho, \quad (9)$$

Therefore, a sliding manifold is defined as follows:

$$\sigma_\rho = gB_\rho - \ddot{\rho}_{ref} + s_\rho, \quad (10)$$

To ensure that the sliding mode is achieved, (10) should lead to (9) in finite time. The derivative of the proposed sliding surface defined in (10) can be rewritten as follows:

$$\dot{\sigma}_{\rho_1} = g \frac{d}{dt} B_{\rho} - \ddot{\rho}_{ref} + \dot{s}_{\rho}, \quad \ddot{\sigma}_{\rho_1} = g \frac{d^2}{dt^2} B_{\rho} - \ddot{\rho}_{ref} + \ddot{s}_{\rho}, \quad (11)$$

where

$$\begin{aligned} \frac{d^2}{dt^2}(B_{\rho}) &= \frac{d}{dt} \left( \frac{d}{dt}(B_{\rho}) \right) \\ &= \frac{d}{dt} \left( \frac{d}{d\varphi}(B_{\rho})\dot{\varphi} + \frac{d}{d\vartheta}(B_{\rho})\dot{\vartheta} + \frac{d}{d\psi}(B_{\rho})\dot{\psi} \right) \\ &= \frac{d(B_{\rho})}{d\varphi}\ddot{\varphi} + \frac{d(B_{\rho})}{d\vartheta}\ddot{\vartheta} + \frac{d(B_{\rho})}{d\psi}\ddot{\psi} + \frac{d}{dt} \left( \frac{d(B_{\rho})}{d\varphi} \right) \dot{\varphi} + \frac{d}{dt} \left( \frac{d(B_{\rho})}{d\vartheta} \right) \dot{\vartheta} + \frac{d}{dt} \left( \frac{d(B_{\rho})}{d\psi} \right) \dot{\psi}. \end{aligned} \quad (12)$$

In the underactuated subsystem,  $\rho(t)$  should follow the desired trajectory  $\rho_{ref}(t)$  in finite time. This can be achieved by enforcing the sliding variable to zero defined in (10). Now,  $\sigma_{\rho}$  is selected as a virtual output and  $U_2$  is the control input.  $\dot{\vartheta}$  is not appeared in (3); therefore, the relative degree is increased, and consequently, another PI-TSMC attractor is defined as follows:

$$\ddot{\sigma}_{\rho} = \dot{\sigma}_{\rho} + \bar{\alpha}_{\rho}\sigma_{\rho} + \bar{\beta}_{\rho} \int_0^t |\sigma_{\rho}|^{\bar{\chi}_{\rho}} \text{sign}(\sigma_{\rho}) d\tau, \quad (13)$$

where  $\bar{\alpha}_{\rho} > \bar{\beta}_{\rho}$  are positive constants.  $\bar{\chi}_{\rho} = \bar{q}_{\rho}/\bar{p}_{\rho}$  with  $\bar{q}_{\rho}$  and  $\bar{p}_{\rho}$  are taken as positive odd numbers [82]. The strong reachability condition for this sliding surface is defined as follows:

$$\dot{\bar{\sigma}}_{\rho} = -\gamma_{1\rho}\bar{\sigma}_{\rho} - \gamma_{2\rho}\text{sign}(\bar{\sigma}_{\rho}), \quad (14)$$

where  $\gamma_{1\rho}$  and  $\gamma_{2\rho}$  are positive constants. Now, consider that the dynamics of an underactuated subsystem are defined by (3); then, the finite time stability of the proposed control law can be analyzed by considering the proposed fast PI-TSMC attractor in (13) and the reaching law given in (15):

$$\begin{aligned} U_2 &= \frac{1}{b_1} \left( \frac{-1}{g \frac{d}{d\varphi}(B_{\rho})} \left( g \left( \frac{d(B_{\rho})}{d\vartheta} \ddot{\vartheta} + \frac{d(B_{\rho})}{d\psi} \ddot{\psi} + \frac{d}{dt} \left( \frac{d(B_{\rho})}{d\vartheta} \right) \dot{\vartheta} + \frac{d}{dt} \left( \frac{d(B_{\rho})}{d\varphi} \right) \dot{\varphi} \right. \right. \right. \\ &\quad \left. \left. + \frac{d}{dt} \left( \frac{d(B_{\rho})}{d\psi} \right) \dot{\psi} \right) + \ddot{s}_{\rho} + \alpha_{\rho_2} \dot{\sigma}_{\rho_1} + \beta_{\rho_2} |\sigma_{\rho_1}|^{\chi_{\rho_2}} \text{sign}(\sigma_{\rho_1}) + \gamma_{\rho_1} \sigma_{\rho_2} \right. \\ &\quad \left. + \gamma_{\rho_2} \text{sign}(\sigma_{\rho_2}) \right) - (a_1 \psi_2 \vartheta_2 + a_2 \bar{\omega} \vartheta_2) \end{aligned} \quad (15)$$

Consequently, the states will converge to their desired equilibria in finite time if the control effort  $U_2$  is chosen as given in (15). To prove this claim, consider the first derivative of (13) w.r.t. time using the dynamics shown in (3) as follows:

$$\begin{aligned} \dot{\bar{\sigma}}_{\rho} &= \ddot{\sigma}_{\rho} + \bar{\alpha}_{\rho} \dot{\sigma}_{\rho} + \bar{\beta}_{\rho} |\sigma_{\rho}|^{\bar{\chi}_{\rho}} \text{sign}(\sigma_{\rho}) \\ &= g \frac{d^2}{dt^2} \hat{B}_{\rho} + \ddot{s}_{\rho} + \alpha_{\rho_2} \dot{\sigma}_{\rho_1} + \beta_{\rho_2} |\sigma_{\rho_1}|^{\chi_{\rho_2}} \text{sign}(\sigma_{\rho_1}) \\ &= g \left( \frac{d(B_{\rho})}{d\varphi} \ddot{\varphi} + \frac{d(B_{\rho})}{d\vartheta} \ddot{\vartheta} + \frac{d(B_{\rho})}{d\psi} \ddot{\psi} + \frac{d}{dt} \left( \frac{d(B_{\rho})}{d\vartheta} \right) \dot{\vartheta} + \frac{d}{dt} \left( \frac{d(B_{\rho})}{d\varphi} \right) \dot{\varphi} \right. \\ &\quad \left. + \frac{d}{dt} \left( \frac{d(B_{\rho})}{d\psi} \right) \dot{\psi} \right) - \ddot{\rho}_{ref} + \dot{s}_{\rho} + \bar{\alpha}_{\rho} \dot{\sigma}_{\rho} + \bar{\beta}_{\rho} |\sigma_{\rho}|^{\bar{\chi}_{\rho}} \text{sign}(\sigma_{\rho}) \end{aligned} \quad (16)$$

$$\dot{\sigma}_{\rho_2} = g \left( \frac{d}{d\vartheta}(\hat{B}_{\rho}) \ddot{\vartheta} + \frac{d}{dt} \left( \frac{d}{d\vartheta}(\hat{B}_{\rho}) \right) \dot{\vartheta} \right) + \ddot{s}_{\rho} + \alpha_{\rho_2} \dot{\sigma}_{\rho_1} + \beta_{\rho_2} |\sigma_{\rho_1}|^{\chi_{\rho_2}} \text{sign}(\sigma_{\rho_1}). \quad (17)$$

Now, the time derivative of Lyapunov candidate functions  $V_\rho = \frac{1}{2}\bar{\sigma}_\rho^2$  is given by (18):

$$\begin{aligned} \dot{V}_\rho = & \bar{\sigma}_\rho \left[ g \left( \frac{d(B_\rho)}{d\varphi} \ddot{\varphi} + \frac{d(B_\rho)}{d\vartheta} \ddot{\vartheta} + \frac{d(B_\rho)}{d\psi} \ddot{\psi} + \frac{d}{dt} \left( \frac{d(B_\rho)}{d\vartheta} \right) \dot{\vartheta} + \frac{d}{dt} \left( \frac{d(B_\rho)}{d\varphi} \right) \dot{\varphi} \right. \\ & + \frac{d}{dt} \left( \frac{d(B_\rho)}{d\psi} \right) \dot{\psi} \Big) + \ddot{s}_\rho + \bar{\alpha}_\rho \dot{\sigma}_\rho + \bar{\beta}_\rho |\bar{\sigma}_\rho|^{\bar{\lambda}_\rho} \text{sign}(\bar{\sigma}_\rho) + \gamma_{1\rho} \bar{\sigma}_\rho \\ & \left. + \gamma_{2\rho} \text{sign}(\bar{\sigma}_\rho) \right] \\ = & \bar{\sigma}_\rho \left[ g \left( \frac{d(B_\rho)}{d\varphi} (F_\varphi + B_\varphi U_2 + \Delta_\varphi) + \frac{d(B_\rho)}{d\vartheta} \ddot{\vartheta} + \frac{d(B_\rho)}{d\psi} \ddot{\psi} + \frac{d}{dt} \left( \frac{d(B_\rho)}{d\vartheta} \right) \dot{\vartheta} \right. \right. \\ & + \frac{d}{dt} \left( \frac{d(B_\rho)}{d\varphi} \right) \dot{\varphi} + \frac{d}{dt} \left( \frac{d(B_\rho)}{d\psi} \right) \dot{\psi} \Big) + \ddot{s}_\rho + \bar{\alpha}_\rho \dot{\sigma}_\rho + \bar{\beta}_\rho |\sigma_\rho|^{\bar{\lambda}_\rho} \text{sign}(\sigma_\rho) \\ & \left. + \gamma_{1\rho} \bar{\sigma}_\rho + \gamma_{2\rho} \text{sign}(\bar{\sigma}_\rho) \right], \end{aligned} \quad (18)$$

where  $B_\varphi = b_1$  and  $F_\varphi = a_1\psi_2\vartheta_2 + a_2\bar{\omega}\vartheta_2$ . Substituting (14) into (18) and rearranging, we get

$$\dot{V}_\rho = -\bar{\sigma}_\rho \left( \gamma_{1\rho} \bar{\sigma}_\rho + \gamma_{2\rho} \text{sign}(\bar{\sigma}_\rho) \right) + \tilde{\Delta}_\phi \leq -\gamma_{1\rho} \bar{\sigma}_\rho^2 - \lambda_\rho |\bar{\sigma}_\rho|, \quad (19)$$

where  $\gamma_{2\rho} - |\tilde{\Delta}_\phi| \geq \lambda_\rho$  and  $|\bar{\sigma}_\rho| = \bar{\sigma}_\rho \text{sign}(\bar{\sigma}_\rho)$ . The inequality in (19) can also be written as follows:

$$\dot{V}_\rho + \eta_{1\rho} V_\rho + \eta_{2\rho} V_\rho^{1/2} \leq 0, \quad (20)$$

where  $\eta_{1\rho} = 2\gamma_{1\rho}$  and  $\eta_{2\rho} = \sqrt{2}\lambda_\rho$ . The extended Lyapunov description in (20) shows the finite time stability of the considered underactuated subsystem via fast PI-TSMC technique. The numerical expression of settling time is derived from (20) in the following form:

$$T_{f\rho} \leq \frac{1}{2\eta_{1\rho}} \ln \left( \frac{\eta_{1\rho} V_\rho^{1/2}(\bar{\sigma}_\rho(0)) + \eta_{2\rho}}{\eta_{2\rho}} \right), \quad (21)$$

236 which guarantees sliding mode convergence of the PI-TSMC in (13) in finite time  $T_{f\rho}$ . The established  
237 sliding mode  $\bar{\sigma}_\rho \rightarrow 0$  will eventually lead to (8), which further confirms the finite time convergence of  
238 tracking error  $e_\rho$  to zero.

The system formulated in (4) demonstrates very similar dynamic structure to those in the systems presented in (3). Thus, the following control law is achieved, which will steer  $\bar{h}$  to  $\bar{h}_{ref}$  and it will also stabilize the  $\vartheta$  dynamic at the origin in finite time.

$$\begin{aligned} U_3 = & \frac{1}{b_2} \left[ \frac{-1}{g \frac{d}{d\vartheta}(B_h)} \left( g \left( \frac{d(B_h)}{d\varphi} \ddot{\varphi} + \frac{d(B_h)}{d\psi} \ddot{\psi} + \frac{d}{dt} \left( \frac{d(B_h)}{d\vartheta} \right) \dot{\vartheta} + \frac{d}{dt} \left( \frac{d(B_h)}{d\varphi} \right) \dot{\varphi} \right. \right. \\ & + \frac{d}{dt} \left( \frac{d(B_h)}{d\psi} \right) \dot{\psi} \Big) + \ddot{s}_h + \bar{\alpha}_h \dot{\sigma}_h + \bar{\beta}_h |\sigma_h|^{\bar{\lambda}_h} \text{sign}(\sigma_h) + \gamma_{1h} \bar{\sigma}_h \\ & \left. + \gamma_{2h} \text{sign}(\bar{\sigma}_h) \right) - (a_3\psi_2\varphi_2 + a_4\bar{\omega}\varphi_2) \Big]. \end{aligned} \quad (22)$$

239 In the next section, the control design for the fully actuated subsystem is presented.

#### 240 4.1.2. Control Design of the Fully Actuated Subsystem

The objective here is to track the performance of the complete system; therefore, the control design of  $z$  and  $\psi$ -dynamics of the quadcopter is presented here. The tracking error of these dynamics is defined as follows:

$$e_z = z_1 - z_{ref}, \quad e_\psi = \psi_1 - \psi_{ref} \quad (23)$$

Since the control law is based on the PI-TSMC attractor, the following variable is defined:

$$\begin{aligned} s_z &= \dot{e}_z + \alpha_z e_z + \beta_z \int_0^t |e_z|^{\chi_z} \text{sign}(e_z) d\tau \\ s_\psi &= \dot{e}_\psi + \alpha_\psi e_\psi + \beta_\psi \int_0^t |e_\psi|^{\chi_\psi} \text{sign}(e_\psi) d\tau \end{aligned} \quad (24)$$

The derivative of (24) is given by the following:

$$\dot{s}_z = \ddot{e}_z + \alpha_z \dot{e}_z + \beta_z |e_z|^{\chi_z} \text{sign}(e_z) \quad (25)$$

$$\begin{aligned} \dot{s}_\psi &= \frac{d}{dt} F(e_\psi, \dot{e}_\psi, |e_\psi|^\chi) = \ddot{e}_\psi + \alpha_\psi \dot{e}_\psi + \beta_\psi |\dot{e}_\psi|^{\chi_\psi} \text{sign}(e_\psi) = \dot{\psi}_2 - \ddot{\psi}_{ref} + (\alpha_1 + \beta_1 |\dot{e}_\psi|^{\chi_1-1}) \dot{e}_\psi \\ &= \alpha_5 \hat{\vartheta}_2 \hat{\varphi}_2 + \beta_3 U_4 - \ddot{\psi}_{ref} + \alpha_{\psi_1} \dot{e}_\psi + \beta_{\psi_1} |\dot{e}_\psi|^{\chi_{\psi_1}} \text{sign}(e_\psi). \end{aligned} \quad (26)$$

After substituting (1), (2), and (23) in (25), we get

$$\begin{aligned} \dot{s}_z &= \ddot{e}_z + \alpha_{z_1} \dot{e}_z + \beta_{z_1} |e_\psi|^{\chi_{z_1}} \text{sign}(e_\psi) \\ &= \dot{z}_2 - \ddot{z}_{ref} + (\alpha_1 + \chi_1 \beta_1 |e_z|^{\chi_1-1}) \dot{e}_z \\ &= -g + b_0 \cos \vartheta_1 \cos \varphi_1 U_1 + \Delta_z - \ddot{z}_{ref} + \alpha_z \dot{e}_z + \beta_z |e_z|^{\chi_z} \text{sign}(e_z). \end{aligned} \quad (27)$$

$$\begin{aligned} \dot{s}_\psi &= \ddot{e}_\psi + \alpha_{\psi_1} \dot{e}_\psi + \beta_{\psi_1} |\dot{e}_\psi|^{\chi_{\psi_1}} \text{sign}(e_\psi) \\ &= \dot{\psi}_2 - \ddot{\psi}_{ref} + (\alpha_1 + \beta_1 |\dot{e}_\psi|^{\chi_1-1}) \dot{e}_\psi \\ &= a_5 \hat{\vartheta}_2 \hat{\varphi}_2 + b_3 U_4 + \Delta_\psi - \ddot{\psi}_{ref} + \alpha_\psi \dot{e}_\psi + \beta_\psi |\dot{e}_\psi|^{\chi_\psi} \text{sign}(e_\psi) \end{aligned} \quad (28)$$

The strong reachability laws is designed as follows:

$$\dot{s}_z = -\gamma_{1z} s_z - \gamma_{2z} \text{sign}(s_z), \quad (29)$$

$$\dot{s}_\psi = -\gamma_{1\psi} s_\psi - \gamma_{2\psi} \text{sign}(s_\psi). \quad (30)$$

Combining (27) and (29) and calculating the control inputs  $U_1$  and  $U_4$ , we get the following:

$$U_1 = \frac{1}{b_0 \cos \vartheta_1 \cos \varphi_1} \left( g - \gamma_{1z} s_z - \gamma_{2z} \text{sign}(s_z) + \ddot{z}_{ref} - \alpha_z \dot{e}_z - \beta_z |e_z|^{\gamma_z} \text{sign}(e_z) \right). \quad (31)$$

$$U_4 = \frac{1}{b_3} \left( -a_5 \hat{\vartheta}_2 \hat{\varphi}_2 - \gamma_{1\psi} s_\psi - \gamma_{2\psi} \text{sign}(s_\psi) + \ddot{\psi}_{ref} - \alpha_\psi \dot{e}_\psi - \beta_\psi |\dot{e}_\psi|^{\gamma_\psi} \text{sign}(e_\psi) \right). \quad (32)$$

These control inputs ensure tracking performance for the  $z$ - and  $\psi$ -dynamics. Now to ensure the sliding mode enforcement in finite time, the dynamics of the fully actuated subsystems defined by (1) and (2) with the PI-TSMC attractor (24), the reaching law (29), and the robust control laws (31) guarantees the finite time enforcement of the sliding mode in the presence of matched uncertainties. To ensure this statement, time derivative of the Lyapunov functions,  $L_z = \frac{1}{2} s_z^2$  and  $L_\psi = \frac{1}{2} s_\psi^2$ , are given by:

$$\begin{aligned} \dot{V}_z &= s_z \left( -g + b_0 \cos \vartheta_1 \cos \varphi_1 U_1 + \Delta_z - \ddot{z}_{ref} + \alpha_z \dot{e}_z + \beta_z |e_z|^{\gamma_z} \text{sign}(e_z) \right) \\ \dot{V}_\psi &= s_\psi \left( a_5 \hat{\vartheta}_2 \hat{\varphi}_2 + b_3 U_4 + \Delta_\psi - \ddot{\psi}_{ref} + \alpha_\psi \dot{e}_\psi + \beta_\psi |\dot{e}_\psi|^{\gamma_\psi} \text{sign}(e_\psi) \right). \end{aligned} \quad (33)$$

Substituting (31) in (33) and then rearranging them, we get:

$$\begin{aligned} \dot{V}_z &= s_z (\Delta_z - \gamma_{1z} s_z - \gamma_{2z} \text{sign}(s_z)) \leq -\gamma_{1z} s_z^2 - \lambda_z |s_z| \\ \dot{V}_\psi &= s_\psi (\Delta_\psi - \gamma_{1\psi} s_\psi - \gamma_{2\psi} \text{sign}(s_\psi)) \leq -\gamma_{1\psi} s_\psi^2 - \lambda_\psi |s_\psi|, \end{aligned} \quad (34)$$

where  $\gamma_{2z} - |\Delta_z| \geq \lambda_z$  and  $\gamma_{2\psi} - |\Delta_\psi| \geq \lambda_\psi$ .

$$\begin{aligned} \dot{V}_z + \bar{\gamma}_{1z} L_z + \bar{\lambda}_z L_z^{1/2} &\leq 0 \\ \dot{V}_\psi + \bar{\gamma}_{1\psi} L_\psi + \bar{\lambda}_\psi L_\psi^{1/2} &\leq 0, \end{aligned} \quad (35)$$

where  $\bar{\gamma}_{1z} = 2\gamma_{1z}$ ,  $\bar{\gamma}_{1\psi} = 2\gamma_{1\psi}$ ,  $\bar{\lambda}_z = \sqrt{2}\lambda_z$ , and  $\bar{\lambda}_\psi = \sqrt{2}\lambda_\psi$ . The settling times are derived from (35) in the following forms:

$$\begin{aligned} T_{f_z} &\leq \frac{1}{2\bar{\gamma}_{1z}} \ln \left( \frac{\bar{\gamma}_{1z} V_z^{1/2}(s_z(0)) + \bar{\lambda}_z}{\bar{\lambda}_z} \right), \\ T_{f_\psi} &\leq \frac{1}{2\bar{\gamma}_{1\psi}} \ln \left( \frac{\bar{\gamma}_{1\psi} V_\psi^{1/2}(s_\psi(0)) + \bar{\lambda}_\psi}{\bar{\lambda}_\psi} \right). \end{aligned} \quad (36)$$

Now, it is evident that as the sliding modes are ensured, the sliding surfaces  $s_z$  and  $s_\psi$  will converge to zero, as well as the error signals  $e_z$  and  $e_\psi \rightarrow 0$  in finite time [46].

#### 4.2. Simulation Results

The nonlinear model of the quadcopter UAV system is simulated in MATLAB®/Simulink 2022a, running on a PC with 11th Gen Intel(R) Core(TM) i5-1135G7 2.40GHz processor using the proposed PI-TSMC control law. The results are obtained for a specific trajectory of the form that involves vertical takeoff along the z-axis and then a circular rotation in the xy plane. Figure 3 shows the tracking performance of the proposed control laws for the quadcopter UAV. The total simulation time is 120 sec and the quadcopter's orientation along x,y and z axis are provided in meters (m). It is considered that all the system states are available to determine the control effort. Moreover, the model parameters are acquired from the existing literature [38].

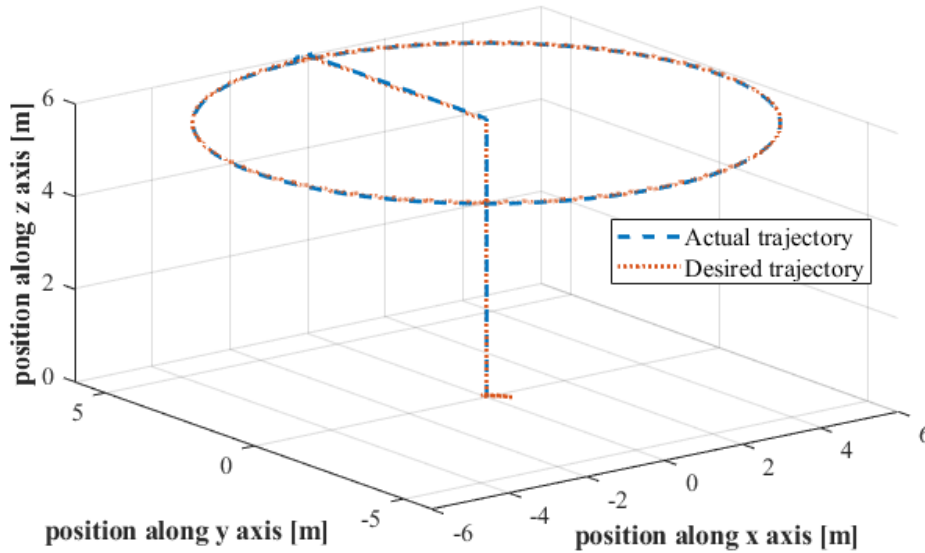
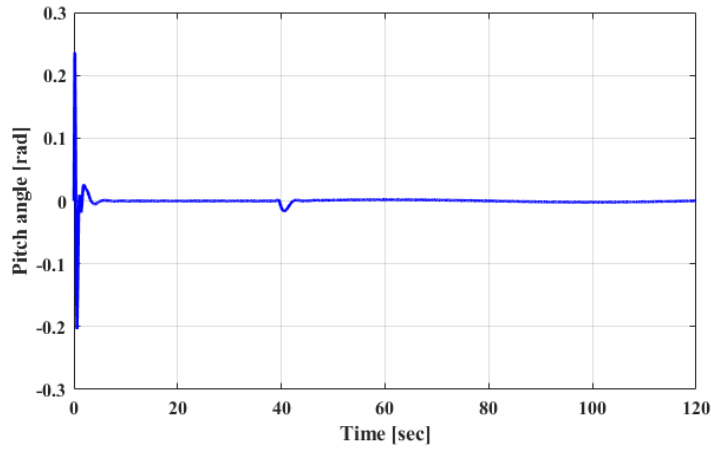
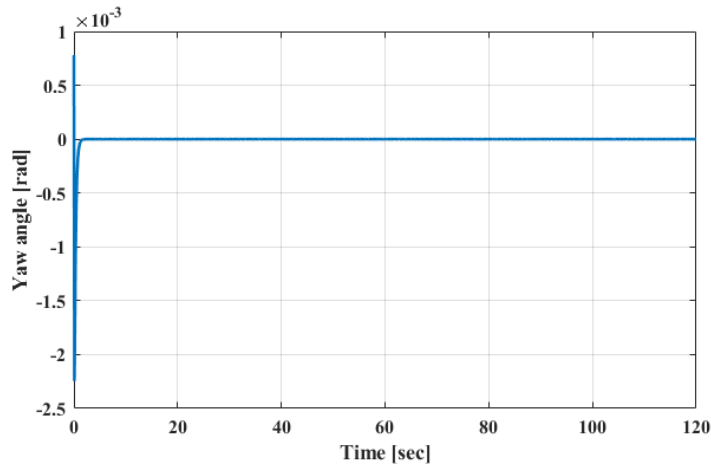


Figure 3. Trajectory tracking using PI-TSMC control technique (circular path).

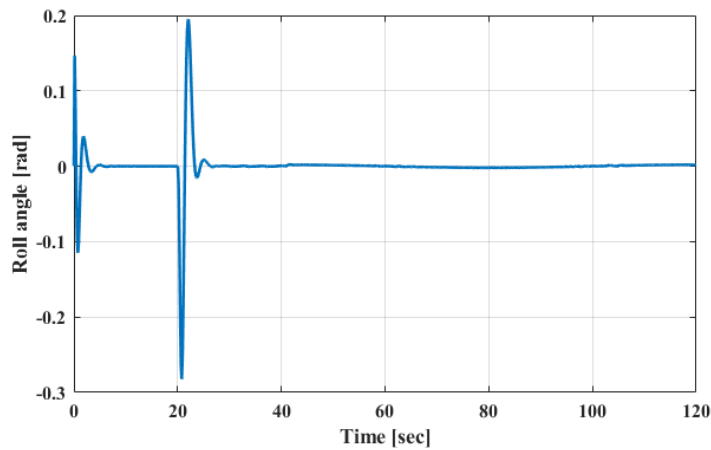
Figure 4 shows the pitch, yaw, and roll angles of the quadcopter measured in radians. With the combination of these angles, the quadcopter can maneuver in all three directions. It can be seen from the results that the proposed control scheme substantially provides a fast converging response with minimum overshoot, guaranteeing the stable maneuvering capabilities of the drone. Furthermore, using this scheme, the undesirable high-frequency chattering effect has been significantly reduced regarding the conventional sliding modes control laws.



(a) Pitch angle



(b) Yaw angle



(c) Roll angle

**Figure 4.** Quadcopter's pitch, yaw, and roll angles during the flight.

258 The control effort required to generate the desired trajectory is presented in Figure 5. The terms  
 259  $U_i$  where  $i = 1 - 4$  represent the control efforts applied to each motor of the UAV. Since the UAV is  
 260 a quadcopter, there will be four motors to generate all types of moments. It can be noticed that the



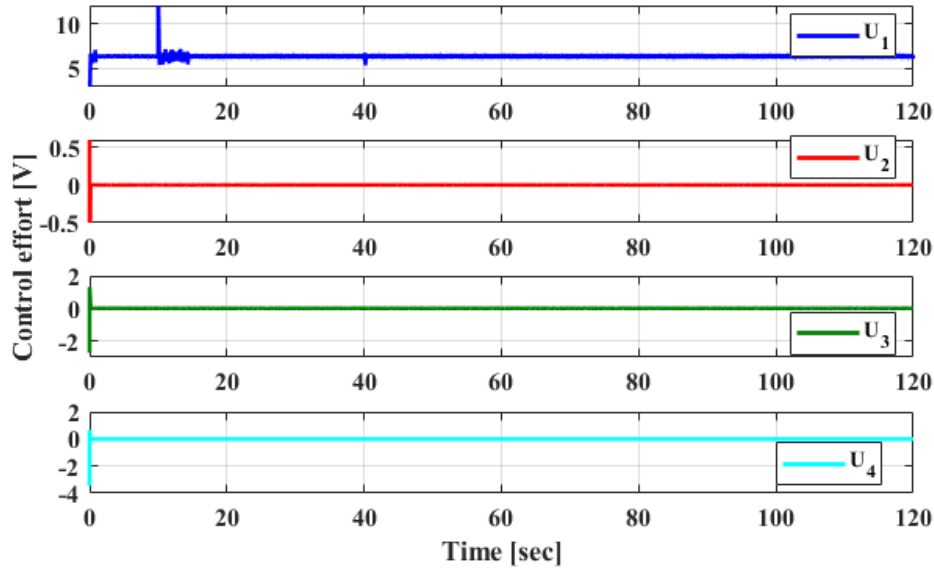


**Figure 5.** Control effort for desired trajectory tracking.

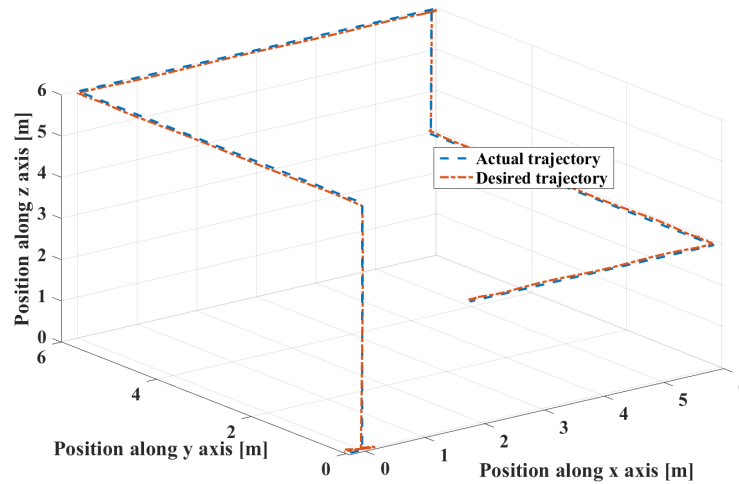


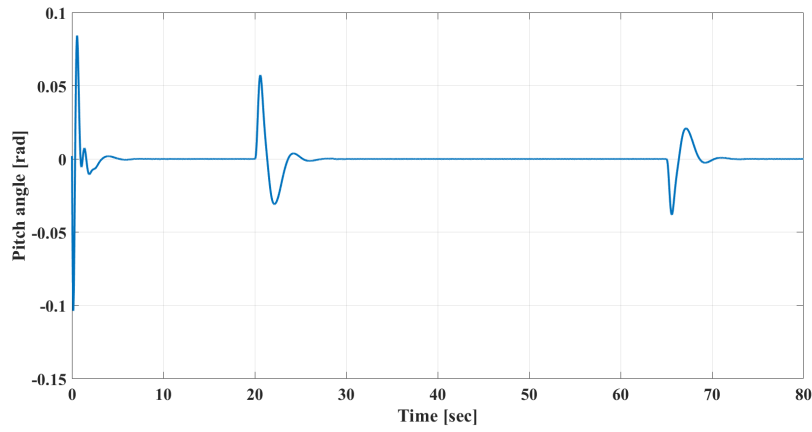
**Figure 6.** Trajectory tracking using PI-TSMC control technique (movement along one axis at a time).

all the control inputs are smooth and have no or minimum chattering. It can also derive the output tracking error to zero in a finite time.

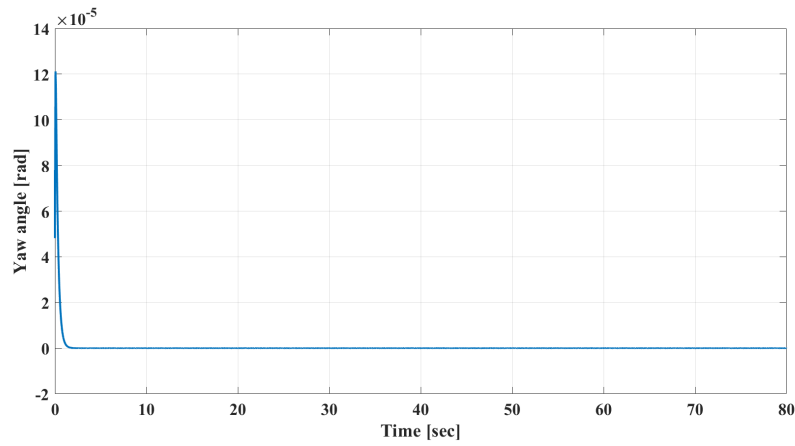
The proposed control law is tested on another trajectory in which the drone take off a reach a certain height and then will move along x and y directions by maintaining that height. The results for the aforementioned trajectory are shown in figure 6. The total simulation time for this trajectory is 80 sec and the quadcopter's orientation along x,y and z axis are provided in meters.

Figure 7 shows the pitch, yaw, and roll angles of the quadcopter measured in radians for the second trajectory shown in figure 6. It can be seen from the results that the proposed control scheme substantially provides a fast-converging response with minimum overshoot, guaranteeing the stable manoeuvring capabilities of the drone. Furthermore, it is evident from figure 7 that to perform different manoeuvring tasks only the pitch (figure 7a) and the roll (figure 7c) angles play a significant role, whereas yaw angle has minimum impact on the manoeuvring capabilities of the drone.

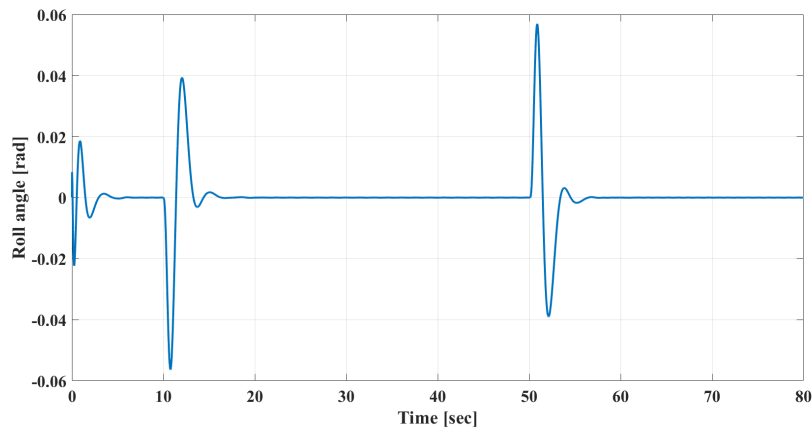
The control effort required to generate the desired trajectory 6 is presented in figure 8. The represent the control efforts applied to each motor of the quadcopter UAV. Since the UAV is a



(a) Pitch angle



(b) Yaw angle



(c) Roll angle

**Figure 7.** Quadcopter's pitch, yaw, and roll angles during the flight (2nd trajectory).

quadcopter, there will be four motors to generate all types of moments and  $U_i$  is the controlled voltage required to generate the trajectory (see figure 6).

## 5. Discussions

With the advent of digitization and augmentation of robotics with AI and related technologies, the oil and gas industry, along with other industries, has started using UAS technology to monitor

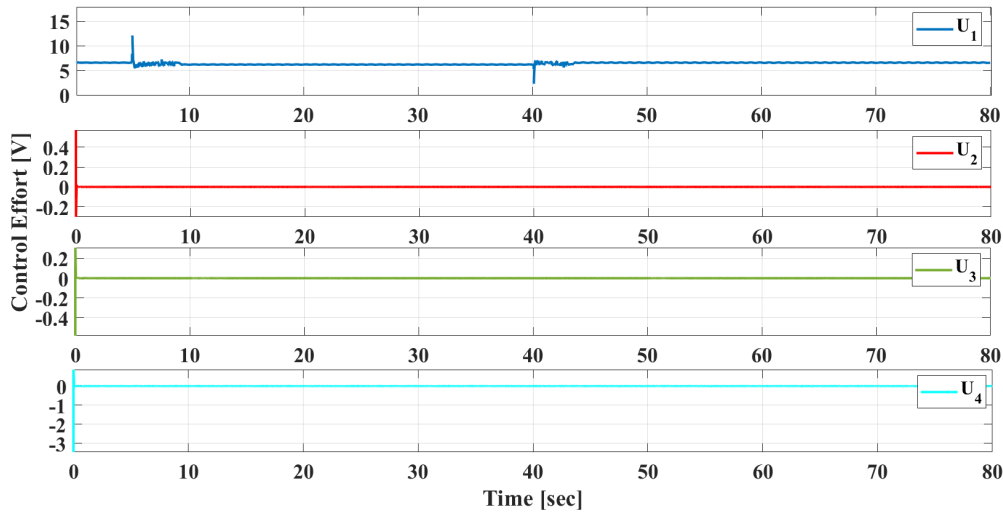


**Figure 8.** Control effort for desired trajectory tracking

these assets. UAS eliminates the need for employees to physically reach difficult areas for inspection and monitoring tasks; the use of gyro-stabilizer cameras attached to these devices allows capturing of high-definition images of inaccessible areas and objects. Furthermore, the data are connected seamlessly to systems that allow data analytics and analysis for pre-programmed assessment of high-value assets.

The focus of this research is to propose a nonlinear robust controller that ensures the stabilized manoeuvring of UAV for pipeline monitoring. Since, the use of UAS is cost-effective and involves a low risk compared to traditional inspection techniques. Moreover, being automatic in nature, it facilitates the periodic regulations of these activities for maintenance, surveillance, and reporting. Although this solution is cost-effective and operation-efficient, there are limitations in the technology, like the limitation of sensor payload, limitation in the flight duration, vulnerability to security attacks, and weather dependency, which make the usage of UAVs challenging.

To overcome these issues the choice of high-capacity batteries with appropriate voltage and discharge rates is very crucial. Lithium Polymer (LiPo) batteries are commonly used for UAVs due to their high energy density. Additionally, ongoing advancements include the development of fuel cell-based UAVs [83] and solar-powered UAVs [84] tailored for particular applications that demand extended flight duration and improved efficiency. On the other hand, it is crucial to note that enhancing flight time often requires trade-offs, which may involve compromising agility or payload capacity. Besides this, other significant emerging UAV implementations in oil and gas sector are found in the integration of AI technology for thermal visualization and methane gas detection, and this trend is expected to drive the UAV service industry in the near future.

## 6. Conclusions

UAVs have emerged as a promising technology for the energy sector, offering a wide range of applications for inspection, monitoring, maintenance, and energy generation. UAS consists of an intelligent UAV, an on-ground controller, and a connection or communication between the controller and the device. The simple setup provides an aerial view of inaccessible and distant locations. The applications of UAVs are widespread due to their ease of use, efficiency, and accurate results. The areas of application of UAVs include both military and nonmilitary domains, including health care, agriculture, photography and filming, and other major industries.

The widespread infrastructure with an inaccessible pipeline network is one of the major challenges when it comes to surveillance, inspection, or emergency response. These major challenges are carried

out safely and efficiently in a cost-effective manner using UAS. However, the effort to make UAVs more suitable in a hostile environment is still a challenging task. Henceforth, a robust control law is derived for a particular class of UAVs, i.e., quadcopter drones. Simulation results are also obtained to evaluate the trajectory tracking performance of the UAV, which shows promising results.

**Funding:** This work was funded by the Deanship of Scientific Research (DSR), University of Jeddah, Saudi Arabia, under Grant No. UJ-02-003-ICGR. The authors, therefore, acknowledge the technical and financial support by the university.

**Conflicts of Interest:** The authors declare no conflict of interest.

## References

- Kitous, A.; Criqui, P.; Bellevrat, E.; Chateau, B. Transformation patterns of the worldwide energy system-scenarios for the century with the POLES model. *The Energy Journal* **2010**, *31*.
- Pickavet, M.; Vereecken, W.; Demeyer, S.; Audenaert, P.; Vermeulen, B.; Develder, C.; Colle, D.; Dhoedt, B.; Demeester, P. Worldwide energy needs for ICT: The rise of power-aware networking. 2008 2nd international symposium on advanced networks and telecommunication systems. IEEE, 2008, pp. 1–3.
- Hänninen, M.; Smedlund, A.; Mitronen, L. Digitalization in retailing: multi-sided platforms as drivers of industry transformation. *Baltic Journal of Management* **2018**.
- Irfan, M.; Iqbal, J.; Iqbal, A.; Iqbal, Z.; Riaz, R.A.; Mehmood, A. Opportunities and challenges in control of smart grids—Pakistani perspective. *Renewable and Sustainable Energy Reviews* **2017**, *71*, 652–674.
- Reali, J. Industry 4.0: how the organizations are evolving from firms to platfirms: a sharing economy insight. Master's thesis, Università Internazionale degli Studi Sociali, LUISS Guido Carli, 2018.
- Van den Ende, J.; Kemp, R. Technological transformations in history: how the computer regime grew out of existing computing regimes. *Research policy* **1999**, *28*, 833–851.
- Weinelt, B.; Knickrehm, M. An introduction to the Digital Transformation of Industries initiative. Technical report, world economic forum, 2018.
- Iqbal, J.; Islam, R.U.; Abbas, S.Z.; Khan, A.A.; Ajwad, S.A. Automating industrial tasks through mechatronic systems—A review of robotics in industrial perspective. *Tehnički vjesnik* **2016**, *23*, 917–924.
- Iizuka, K.; Itoh, M.; Shiodera, S.; Matsubara, T.; Dohar, M.; Watanabe, K. Advantages of unmanned aerial vehicle (UAV) photogrammetry for landscape analysis compared with satellite data: A case study of postmining sites in Indonesia. *Cogent Geoscience* **2018**, *4*, 1498180.
- Böhm, F.; Schulte, A. UAV autonomy research-challenges and advantages of a fully distributed system architecture. International Foundation for Telemetering, 2012.
- Choi, J.; Kimb, D.B. A new UAV-based module lifting and transporting method: Advantages and challenges. Vol. 36 of Proc., Int. Symp. on Automation and Robotics in Construction ISARC, 2019, pp. 645–650.
- Almagbile, A. Estimation of crowd density from UAVs images based on corner detection procedures and clustering analysis. *Geo-spatial Information Science* **2019**, *22*, 23–34.
- Novák, D.; Čermák, P. Advantages of using multi-agent principles in FAIL-SAFE UAV system design. 2011 16th International Conference on Methods & Models in Automation & Robotics. IEEE, 2011, pp. 162–167.
- Saadatseresht, M.; Hashempour, A.; Hasanlou, M. UAV photogrammetry: a practical solution for challenging mapping projects. *The International Archives of Photogrammetry, Remote Sensing and Spatial Information Sciences* **2015**, *40*, 619.
- Cevik, P.; Kocaman, I.; Akgul, A.S.; Akca, B. The small and silent force multiplier: a swarm UAV—electronic attack. *Journal of Intelligent & Robotic Systems* **2013**, *70*, 595–608.
- Tvaryanas, A.P. Visual scan patterns during simulated control of an uninhabited aerial vehicle (UAV). *Aviation, space, and environmental medicine* **2004**, *75*, 531–538.
- Rodriguez, P.A.; Geckle, W.J.; Barton, J.D.; Samsundar, J.; Gao, T.; Brown, M.Z.; Martin, S.R. An emergency response UAV surveillance system. AMIA Annual Symposium Proceedings. American Medical Informatics Association, 2006, Vol. 2006, p. 1078.
- Lagkas, T.; Argyriou, V.; Bibi, S.; Sarigiannidis, P. UAV IoT framework views and challenges: towards protecting drones as “things”. *Sensors* **2018**, *18*, 4015.

19. Paredes, J.A.; Acevedo, J.; Mogrovejo, H.; Villalta, J.; Furukawa, R. Quadcopter design for medicine transportation in the peruvian amazon rainforest. 2016 IEEE XXIII international congress on electronics, electrical engineering and computing (INTERCON). IEEE, 2016, pp. 1–6.
20. Gu, H.; Lyu, X.; Li, Z.; Shen, S.; Zhang, F. Development and experimental verification of a hybrid vertical take-off and landing (VTOL) unmanned aerial vehicle (UAV). 2017 International Conference on Unmanned Aircraft Systems (ICUAS). IEEE, 2017, pp. 160–169.
21. Majumdar, J.; Vinay, S.; Selvi, S. Registration and mosaicing for images obtained from UAV. 2004 International Conference on Signal Processing and Communications, 2004. SPCOM'04. IEEE, 2004, pp. 198–203.
22. Puri, A. A survey of unmanned aerial vehicles (UAV) for traffic surveillance. *Department of computer science and engineering, University of South Florida* **2005**, pp. 1–29.
23. Valentino, R.; Jung, W.S.; Ko, Y.B. A design and simulation of the opportunistic computation offloading with learning-based prediction for unmanned aerial vehicle (uav) clustering networks. *Sensors* **2018**, *18*, 3751.
24. Orfanus, D.; de Freitas, E.P.; Eliassen, F. Self-organization as a supporting paradigm for military UAV relay networks. *IEEE Communications Letters* **2016**, *20*, 804–807.
25. Cho, J.; Lim, G.; Biobaku, T.; Kim, S.; Parsaei, H. Safety and security management with unmanned aerial vehicle (UAV) in oil and gas industry. *Procedia manufacturing* **2015**, *3*, 1343–1349.
26. Markets.; Markets. Pipeline transportation market by solution (security solutions, automation and control, integrity and tracking solutions, network communication solutions, and other), by modes (oil and gas, coal, chemical, water, and other)—global forecast to 2019. <http://www.marketsandmarkets.com/Market-Reports/pipeline-transportation-market-110375125.html>, 2014, accessed August 8, 2020.
27. Shukla, A.; Karki, H. Application of robotics in onshore oil and gas industry—A review Part I. *Robotics and Autonomous Systems* **2016**, *75*, 490–507.
28. Papadakis, G.A. Major hazard pipelines: a comparative study of onshore transmission accidents. *Journal of Loss Prevention in the Process Industries* **1999**, *12*, 91–107.
29. Gómez, C.; Green, D.R. Small unmanned airborne systems to support oil and gas pipeline monitoring and mapping. *Arabian Journal of Geosciences* **2017**, *10*, 202.
30. Um, J.S.; Wright, R. Pipeline construction and reinstatement monitoring: current practice, limitations and the value of airborne videography. *Science of the total environment* **1996**, *186*, 221–230.
31. Titus, S. *Proposed Methods for a Phase I Cultural Resources Survey of the Keystone Pipeline Project Corridor, Cushing Extension, Oklahoma Segment, Kay, Noble, and Payne Counties*; Oklahoma, 2007.
32. Koh, L.P.; Wich, S.A. Dawn of drone ecology: low-cost autonomous aerial vehicles for conservation. *Tropical conservation science* **2012**, *5*, 121–132.
33. news letter, D. commercial drone data opening up new opportunities for industrial applications. <https://www.dji.com/newsroom/news/blog-commercial-drone-data-opening-up-new-opportunities>, 2019, accessed August 7, 2020.
34. English, D.; others. Improving Asset Management at Process Plants Through UAV (Unmanned Aerial Vehicle) Inspections. Abu Dhabi International Petroleum Exhibition and Conference. Society of Petroleum Engineers, 2015.
35. Ham, Y.; Han, K.K.; Lin, J.J.; Golparvar-Fard, M. Visual monitoring of civil infrastructure systems via camera-equipped Unmanned Aerial Vehicles (UAVs): a review of related works. *Visualization in Engineering* **2016**, *4*, 1.
36. Ducard, G.J. *Fault-tolerant flight control and guidance systems: Practical methods for small unmanned aerial vehicles*; Springer Science & Business Media, 2009.
37. Aljuaid, K.G.; Albuoderman, M.A.; AlAhmadi, E.A.; Iqbal, J. Comparative Review of Pipelines Monitoring and Leakage Detection Techniques. 2020 2nd International Conference on Computer and Information Sciences (ICCIS). IEEE, 2020, pp. 1–6.
38. Ullah, S.; Mehmood, A.; Khan, Q.; Rehman, S.; Iqbal, J. Robust Integral Sliding Mode Control Design for Stability Enhancement of Under-actuated Quadcopter. *International Journal of Control, Automation and Systems* **2020**, pp. 1–08.

39. Mechali, O.; Xu, L.; Xie, X.; Iqbal, J. Fixed-time nonlinear homogeneous sliding mode approach for robust tracking control of multirotor aircraft: Experimental validation. *Journal of the Franklin Institute* **2022**, *359*, 1971–2029.
40. Khan, S.; Bendoukha, S.; Naeem, W.; Iqbal, J. Experimental validation of an integral sliding mode-based LQG for the pitch control of a UAV-mimicking platform. *Advances in Electrical and Electronic Engineering* **2019**, *17*, 275–284.
41. Wasim, M.; Ullah, M.; Iqbal, J. Gain-scheduled proportional integral derivative control of taxi model of unmanned aerial vehicles. *Revue Roumaine des Sciences Techniques-Serie Electrotechnique et Energetique* **2019**, *64*, 75–80.
42. Labbadi, M.; Iqbal, J.; Djemai, M.; Boukal, Y.; Bouteraa, Y. Robust tracking control for a quadrotor subjected to disturbances using new hyperplane-based fast Terminal Sliding Mode. *Plos one* **2023**, *18*, e0283195.
43. Advanced Research with Autonomous Unmanned Aerial Vehicles.
44. Butt, M.; Munawar, K.; Bhatti, U.I.; Iqbal, S.; Al-Saggaf, U.M.; Ochieng, W. 4D trajectory generation for guidance module of a UAV for a gate-to-gate flight in presence of turbulence. *International Journal of Advanced Robotic Systems* **2016**, *13*, 125.
45. Mechali, O.; Xu, L.; Xie, X.; Iqbal, J. Theory and practice for autonomous formation flight of quadrotors via distributed robust sliding mode control protocol with fixed-time stability guarantee. *Control Engineering Practice* **2022**, *123*, 105150.
46. Ullah, S.; Khan, Q.; Mehmood, A.; Kirmani, S.A.M.; Mechali, O. Neuro-adaptive fast integral terminal sliding mode control design with variable gain robust exact differentiator for under-actuated quadcopter UAV. *ISA transactions* **2022**, *120*, 293–304.
47. Zatout, M.S.; Rezoug, A.; Rezoug, A.; Baizid, K.; Iqbal, J. Optimisation of fuzzy logic quadrotor attitude controller–particle swarm, cuckoo search and BAT algorithms. *International Journal of Systems Science* **2022**, *53*, 883–908.
48. Watts, A.C.; Ambrosia, V.G.; Hinkley, E.A. Unmanned aircraft systems in remote sensing and scientific research: Classification and considerations of use. *Remote Sensing* **2012**, *4*, 1671–1692.
49. Villa, T.F.; Gonzalez, F.; Miljevic, B.; Ristovski, Z.D.; Morawska, L. An overview of small unmanned aerial vehicles for air quality measurements: Present applications and future perspectives. *Sensors* **2016**, *16*, 1072.
50. Brady, J.M.; Stokes, M.D.; Bonnardel, J.; Bertram, T.H. Characterization of a quadrotor unmanned aircraft system for aerosol-particle-concentration measurements. *Environmental science & technology* **2016**, *50*, 1376–1383.
51. kalpa Gunarathna, J.; Munasinghe, R. Development of a quad-rotor fixed-wing hybrid unmanned aerial vehicle. 2018 Moratuwa Engineering Research Conference (MERCon). IEEE, 2018, pp. 72–77.
52. Schuyler, T.J.; Guzman, M.I. Unmanned aerial systems for monitoring trace tropospheric gases. *Atmosphere* **2017**, *8*, 206.
53. Inaudi, D.; Glisic, B. Long-range pipeline monitoring by distributed fiber optic sensing. *Journal of pressure vessel technology* **2010**, *132*.
54. Almazyad, A.S.; Seddiq, Y.M.; Alotaibi, A.M.; Al-Nasheri, A.Y.; BenSaleh, M.S.; Obeid, A.M.; Qasim, S.M. A proposed scalable design and simulation of wireless sensor network-based long-distance water pipeline leakage monitoring system. *Sensors* **2014**, *14*, 3557–3577.
55. Krohn, D.A.; MacDougall, T.; Mendez, A. *Fiber optic sensors: fundamentals and applications*; Spie Press Bellingham, WA, 2014.
56. Razzaq, S.; Xydeas, C.; Mahmood, A.; Ahmed, S.; Ratyal, N.I.; Iqbal, J. Efficient optimization techniques for resource allocation in UAVs mission framework. *PloS one* **2023**, *18*, e0283923.
57. Green, D.R.; Gomez, C. Small-scale airborne platforms for oil and gas pipeline monitoring and mapping. Proceedings of the Marine and Coastal Environments Conference-San Diego, US (October 1998), 1998, pp. 1–54.
58. Emel'yanov, S.; Makarov, D.; Panov, A.I.; Yakovlev, K. Multilayer cognitive architecture for UAV control. *Cognitive Systems Research* **2016**, *39*, 58–72.
59. Caltabiano, D.; Muscato, G.; Orlando, A.; Federico, C.; Giudice, G.; Guerrieri, S. Architecture of a UAV for volcanic gas sampling. 2005 IEEE Conference on Emerging Technologies and Factory Automation. IEEE, 2005, Vol. 1, pp. 6–pp.



60. Tisdale, J.; Ryan, A.; Zennaro, M.; Xiao, X.; Caveney, D.; Rathinam, S.; Hedrick, J.K.; Sengupta, R. The software architecture of the Berkeley UAV platform. 2006 IEEE Conference on Computer Aided Control System Design, 2006 IEEE International Conference on Control Applications, 2006 IEEE International Symposium on Intelligent Control. IEEE, 2006, pp. 1420–1425.
61. Pastor, E.; Lopez, J.; Royo, P. UAV payload and mission control hardware/software architecture. *IEEE Aerospace and Electronic Systems Magazine* **2007**, *22*, 3–8.
62. Zhou, Y.; Cheng, N.; Lu, N.; Shen, X.S. Multi-UAV-aided networks: Aerial-ground cooperative vehicular networking architecture. *IEEE Vehicular Technology Magazine* **2015**, *10*, 36–44.
63. Zhang, Q.; Jiang, M.; Feng, Z.; Li, W.; Zhang, W.; Pan, M. IoT enabled UAV: Network architecture and routing algorithm. *IEEE Internet of Things Journal* **2019**, *6*, 3727–3742.
64. Boubeta-Puig, J.; Moguel, E.; Sánchez-Figueroa, F.; Hernández, J.; Preciado, J.C. An autonomous UAV architecture for remote sensing and intelligent decision-making. *IEEE Internet Computing* **2018**, *22*, 6–15.
65. Gancet, J.; Hattenberger, G.; Alami, R.; Lacroix, S. Task planning and control for a multi-UAV system: architecture and algorithms. 2005 IEEE/RSJ International Conference on Intelligent Robots and Systems. IEEE, 2005, pp. 1017–1022.
66. Rathinam, S.; Zennaro, M.; Mak, T.; Sengupta, R. An architecture for UAV team control. Proc. IFAC Conference on Intelligent Autonomous Vehicles in Portugal, 2004.
67. Azari, M.M.; Rosas, F.; Chen, K.C.; Pollin, S. Ultra reliable UAV communication using altitude and cooperation diversity. *IEEE Transactions on Communications* **2017**, *66*, 330–344.
68. Gupta, L.; Jain, R.; Vaszkun, G. Survey of important issues in UAV communication networks. *IEEE Communications Surveys & Tutorials* **2015**, *18*, 1123–1152.
69. Dickmanns, E.D. A general dynamic vision architecture for UGV and UAV. *Applied Intelligence* **1992**, *2*, 251–270.
70. Themistocleous, K. The use of UAV platforms for remote sensing applications: case studies in Cyprus. Second International Conference on Remote Sensing and Geoinformation of the Environment (RSCy2014). International Society for Optics and Photonics, 2014, Vol. 9229, p. 92290S.
71. Kada, B.; Munawar, K.; Shaikh, M.; Hussaini, M.; Al-Saggaf, U. UAV attitude estimation using nonlinear filtering and low-cost mems sensors. *IFAC-PapersOnLine* **2016**, *49*, 521–528.
72. Frey, J.; Kovach, K.; Stemmler, S.; Koch, B. UAV photogrammetry of forests as a vulnerable process. A sensitivity analysis for a structure from motion RGB-image pipeline. *Remote Sensing* **2018**, *10*, 912.
73. Pajares, G. Overview and current status of remote sensing applications based on unmanned aerial vehicles (UAVs). *Photogrammetric Engineering & Remote Sensing* **2015**, *81*, 281–330.
74. Hassan, A. Review of the global oil and gas industry: a concise journey from ancient time to modern world. *Petroleum Technology Development Journal* **2013**, *3*, 123–141.
75. Bastianoni, S.; Campbell, D.; Susani, L.; Tiezzi, E. The solar transformity of oil and petroleum natural gas. *Ecological Modelling* **2005**, *186*, 212–220.
76. Bangsund, D.A.; Leistritz, F.L. Economic contribution of the petroleum industry to North Dakota. Technical report, 2007.
77. Bajpai, S.; Gupta, J. Securing oil and gas infrastructure. *Journal of Petroleum Science and Engineering* **2007**, *55*, 174–186.
78. Udie, J.; Bhattacharyya, S.; Ozawa-Meida, L. A conceptual framework for vulnerability assessment of climate change impact on critical oil and gas infrastructure in the niger delta. *Climate* **2018**, *6*, 11.
79. Mohamed, N.; Al-Jaroodi, J.; Jawhar, I.; Noura, H.; Mahmoud, S. UAVFog: A UAV-based fog computing for Internet of Things. 2017 IEEE SmartWorld, Ubiquitous Intelligence & Computing, Advanced & Trusted Computed, Scalable Computing & Communications, Cloud & Big Data Computing, Internet of People and Smart City Innovation (SmartWorld/SCALCOM/UIC/ATC/CBDCom/IOP/SCI). IEEE, 2017, pp. 1–8.
80. Koldaev, A.V. Non-military UAV applications. Aero India International Seminar-2007 Edition. Bangalore. Citeseer, 2007.
81. Toro, F.G.; Tsourdos, A. *UAV or Drones for Remote Sensing Applications*; MDPI-Multidisciplinary Digital Publishing Institute, 2018.
82. Yu, X.; Feng, Y.; Man, Z. Terminal sliding mode control—An overview. *IEEE Open Journal of the Industrial Electronics Society* **2020**, *2*, 36–52.

83. Prajapati, S.; Charulatha, S. Design of a PEM fuel cell powered autonomous quadcopter. *International Journal of Modelling, Identification and Control* **2023**, *42*, 271–286.
84. Kingry, N.; Towers, L.; Liu, Y.C.; Zu, Y.; Wang, Y.; Staheli, B.; Katagiri, Y.; Cook, S.; Dai, R. Design, modeling and control of a solar-powered quadcopter. 2018 IEEE International Conference on Robotics and Automation (ICRA). IEEE, 2018, pp. 1251–1258.

© 2023 by the authors. Submitted to *Drones* for possible open access publication under the terms and conditions of the Creative Commons Attribution (CC BY) license (<http://creativecommons.org/licenses/by/4.0/>).